Model-Based Estimation of Functional Connectivity in Whole-Brain Multifiber Implant Calcium Dynamics in Behaving Mice

Report for 2019 Computational Psychiatry Course

Aleksejs Fomins

June 8, 2019

1 Introduction

Mesoscopic whole-brain imaging is a large field. A wide variety of measurement techniques, such as fMRI [29, 5, 7, 6, 22], EEG [44, 3, 15, 21] and wide-field calcium imaging [12, 36, 17, 8] are used to record functions of neuronal signals averaged over large neuronal populations. An important question is the capacity of recorded mesoscopic signals to explain observables external to the brain, such as sensory input, behaviour and learning, and vice versa.

An ideal latent variable model would be capable of accurately predicting the future values of mesoscopic activity and external observables based their past values. Given current state of the art data, the construction of a fully self-consistent mesoscopic model of a brain or its part is unlikely because, among others, such a model would struggle to account for a) heterogeneity of a neuronal population b) specificity of its response c) inputs from unobserved neuronal populations and external stimuli. However, it is not unreasonable to assume that brain activity can be decomposed into a spatio-temporal basis of increasing detail, allowing to have a progressively more accurate account of external observables.

An interesting latent variable of a network activity is the so-called Functional Connectivity [11, 18]. Loosely, it can be defined as the capacity of the value of one variable to be predictive of the value of another variable at a later time. FC is designed to indicate potential causal relationships between variables, however, far greater knowledge of the system is required to guarantee causality as the only possible explanation of FC [43]. While it is frequently impossible to unambiguously estimate FC [43], standardized metrics of FC have been demonstrated to be predictive of working memory [13, 9], daydreaming [23], decision making [25], pathology [33] and learning [4]. Among others, the following model-free metrics for FC have been proposed: correlation [14, 39, 42], coherence [30], Granger Causality [45, 2, 40, 35], KL-Divergence [1, 27], Transfer Entropy [43, 41, 28, 24, 25, 19, 34], Topological Causality [16].

FC is a direct measure of the information propagation in the system. It can be used to infer the direction of information propagation, as well as the sinks and sources of information in a given dynamical system. Further, unlike anatomical connectivity, FC need not be constant even on the short time scales. A fastly changing FC can indicate at multipartite nature of the underlying nodes and at distinct rules which determine whether a given connection is active in a given context.

Our ultimate goal is to compare the performance of model-free and model-based estimators of FC on simulated data, as well as the real data of whole-brain calcium imaging. This report will present current progress in application of model-based techniques, namely MAR [31] and DCM [37, 11, 10, 20]. In the following publication, we intend to finish the DCM analysis started in this work, and compare it to model-free analysis using correlation, MI and TE.

2 Data

In this study, we analyse the recent data gathered using a novel multifiber implant technology [38]. The advantage of this technique compared to previous approaches is the ability to simultaneously image multiple cortical and subcortical areas with high selectivity, while benefiting from high temporal resolution of calcium indicators. In particular, fluorescence signals from GCaMP6f-expressing mice were recorded at 20Hz using chronic implants of multifiber arrays of 12 to 48 channels. During a period of 12-18 days mice would perform a texture discrimination task for an average of 400 trials. Each trial lasts 8s. During each trial a mouse must use tactile information to discriminate between two randomly presented textures and report by licking or not licking at a provided water port. Correct classification is water-rewarded and wrong is punished by white noise. Performance during each

(a) Example Z-Scored Neuronal Trace

(b) Example Lick Rate

(c) Example paw movement amplitude
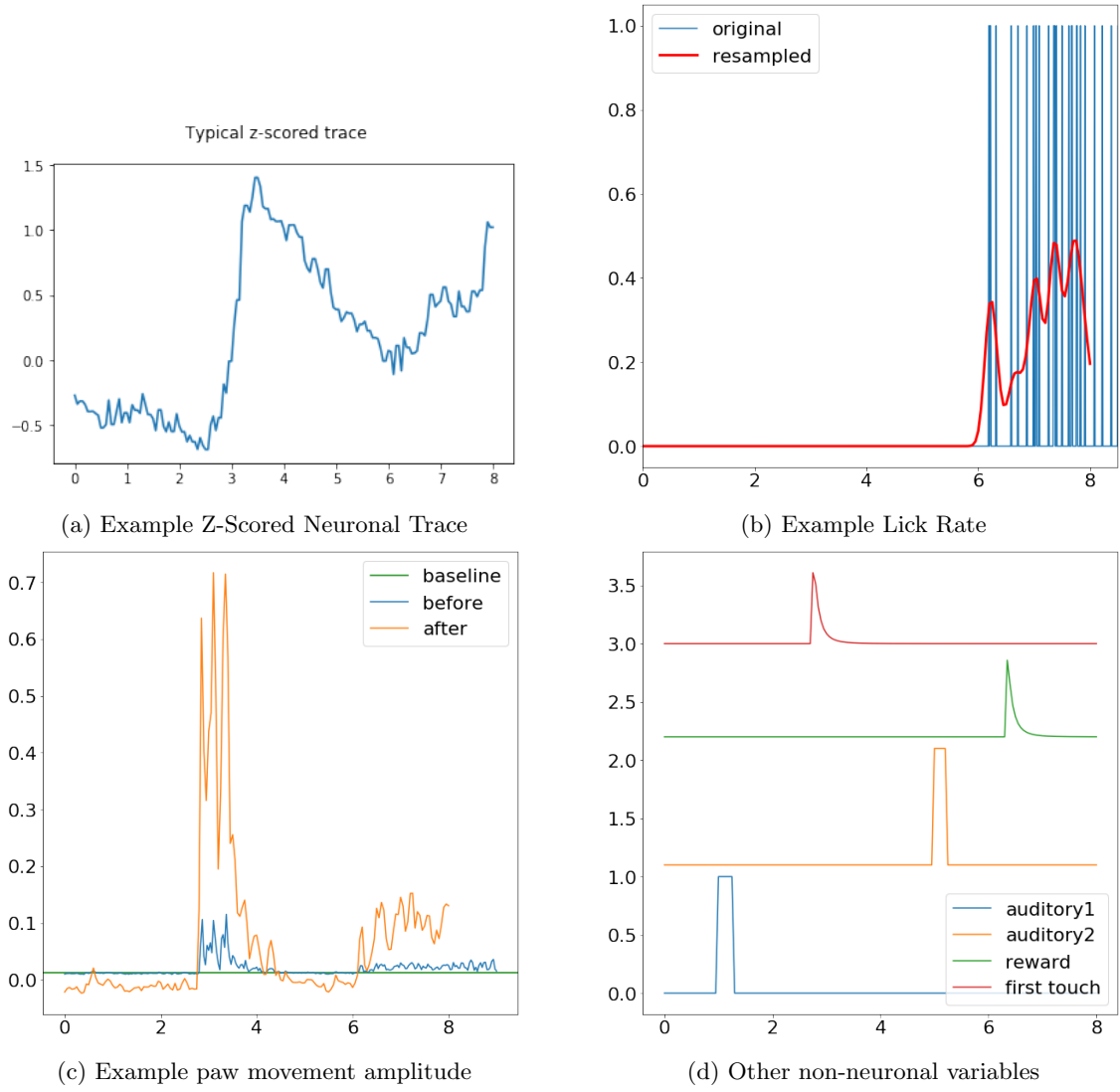
(d) Other non-neuronal variables

Figure 1: Example behavioural and neuronal data during a typical 8 second trial (x-axis), resampled to neuronal sampling frequency of 20Hz and normalized across all trials

trial is classified into 4 categories (Go, NoGo, Miss, False Alarm) based on correct vs actual outcome. Behavioural and external variables [fig. 1], such as paw movement, lick rate, whisking angle, distance to texture, start and finish auditory cues, time to first touch, first lick and reward are also recorded. For the purpose of this study, we have resampled the behavioural and external variables to match the neuronal sampling frequency. Also, single time step data, such as reward time, have been convolved with a log-exponential distribution to mimic a realistic time-response.

3   Preliminary Exploratory Analysis

We believe that it is advantageous to get familiar with the data using simple well-established metrics prior to using sophisticated model-based explanations, mainly to obtain intuition on whether the data is consistent with the assumptions of the models we later intend to fit. Firstly, we expect the measured neuronal signal to be autocorrelated, since the GCaMP6f timescale of 500ms is larger than the sampling timestep of 50ms. Secondly, we expect the signals from different brain areas to be cross-correlated. Since the slowly-changing components of the signals can be linearised to a reasonable accuracy within the range of a few time steps, a zero cross-correlation would indicate that any coupling between channels is purely nonlinear and very weak compared to the signal magnitude.

As expected, the autocorrelation of the data resembles a decaying exponential function, indicating the presence of a slowly changing component [fig. 2a]. Further, the autocorrelation has an oscillatory component which is typical of a fastly changing signal convolved with a slowly decaying exponential. The cross-correlation of the data indicates clustering, as some channels are highly correlated to each other while not being correlated to other channels [figs. 2b

(a) Example value of autocorrelation of neuronal signal from a single channel

(b) Example value of cross-correlation between channels of a 12 channel mouse

(c) Example delay of cross-correlation between channels of a 12 channel mouse

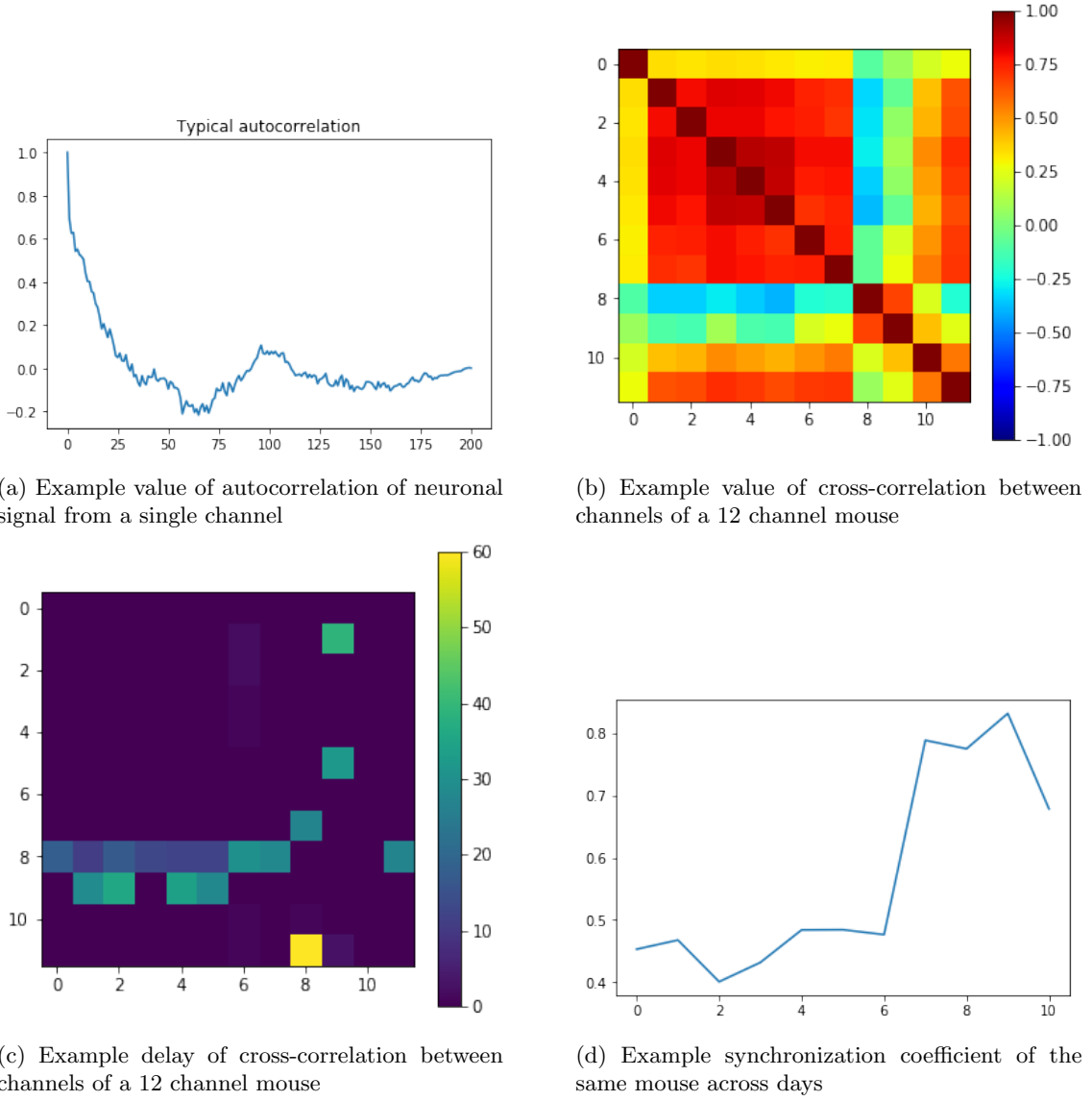(d) Example synchronization coefficient of the same mouse across days

Figure 2: Preliminary analysis of neuronal data

and 2c]. In some cases, we observe a channel that is somewhat correlated to all other channels, while other channels are not correlated, indicating a propagation of some global brain state. Further, we decided to investigate how cross-correlation changes with learning. For this purpose, we define the synchronization coefficient as the average absolute value of the off-diagonal entries of the channel correlation matrix C_{ij}

$$S = \frac{1}{N^2 - N} \sum_{ij} |C_{ij}| - \delta_{ij} \tag{1}$$

and plot it as a function of the training day [fig. 2d]. We see that the average synchronization between channels is 0.5, meaning that the data is highly correlated. Further, in several mice we observe a steep rise of synchronization to values of 0.8 or even 0.9 a few days after they have achieved expert level performance. This does not happen to all animals that reach expert level performance, so we are looking forwards to further investigate this observation in later works.

4   MAR Model

We have considered the following form of an autoregressive process

$$X_i(t) = \sum_{j=1}^{p} \sum_{k=1}^{N_X} A_{ik}^j X_k(t - j) + \sum_{k=1}^{N_U} B_{ik} U_k(t - 1) + \epsilon_i \tag{2}$$

3

where X is the observed calcium signal, U is the external input, p is the maximal order of the MAR model, A and B are the unknown functional connectivity tensors. In this study we have investigated 3 different implementations of the above model: analytic unconstrained solution, numeric constrained and regularized solution and a bayesian model inversion framework by Penny et al [31]. In table 1 we present the comparison between features available in each implementation. Note that many of the features not present in the below table are reasonably easy to implement. We had to restrict ourselves only to the features that form the essential differences between the 3 implementations in order to be time-efficient. For the analytic and numeric model we derived and implemented an optimized solver for scratch. The reason not to use an existing library was the inability of libraries we found to handle fitting a MAR model to multiple trials simultaneously, which we believe is necessary to improve rigor of the estimated model parameters. The difference of the numerical model to the analytic was in additional L_1 regularization and a constraint requiring all A matrix elements to be non-negative. We have chosen this constraint because all of the measured neuronal populations are excitatory. Most elements in an unconstrained estimated A matrix are positive, and those that are negative are relativelty small, so we concluded that there is likely no real inhibitory effect between populations, and it makes sense to restrict it altogether. Finally, we have also used a Bayesian inversion-based MAR model implemented by Penny et el. [31] as part of the SPM toolbox. This model makes prior assumptions about the distributions of model parameters (A matrix elements), their precisions, as well as the precisions of the added noise. Penny et al. [31] then proceed to invert the model using VB mean-field approximation, obtaining an iterative procedure for computing the model parameters and the associated model evidences.

	Analytic	Numeric	Bayesian
Arbitrary model order	Yes	No	Yes
External input	Yes	No	No
Optimization over trials	Yes	Yes	No
Non-negative constraint	No	Yes	No
Regularization	No	Yes	Yes
Model Selection Criteria	AIC,BIC	AIC,BIC	ME

Table 1: Feature comparison between the 3 MAR models used

We summarize the results of the above model estimates as follows

- The A matrix estimates for all model orders are diagonally-dominant, with $p = 1$ being the most dominant order. This means that a large portion of a neuronal signal can be explained by its own past value. This is not surprising given the autocorrelation we have observed previously, and is expected of the slowly-decaying calcium indicator signals.

- The A matrix estimates experience small changes in presence of the external observables U, but qualitatively they stay diagonally-dominant [figs. 5a and 5b].

- Similarly, the A matrix estimate appears qualitatively the same when computed separately for each performance class (Go, Nogo, Miss, False Alarm) [fig. 7]

- The A matrix estimates based on Bayesian inversion appear to have stronger off-diagonal entries than the other methods [fig. 5c]. It is hard to judge whether this estimate is more accurate than that of the analytic models. On one hand, the Bayesian model starts with the diagonal prior for the A matrix, so having more off-diagonal entries in not the result of a local minima. From the other, it has more rigorous estimation of the noise covariance which would in principle make it more accurate. However, unlike our analytic estimate, it has a downside of not being able to combine all trials into one estimate, which dramatically reduces the amount of data points available to the method compared to the analytic one, potentially resulting in spurious connections due to noise fitting.

- The A matrix estimates based on numeric regularized approach demonstrate comparable model fitness while having most entries set to zero [fig. 5d]. Interestingly, many diagonal entries are zero, suggesting that the signal of the associated channels can be to some extent explained by other channels. In particular, it is clearly visible that channel 3 correlates with all other channels, indicating some sort of whole-brain activity.

- Input matrix U appears quite informative [fig. 6]. For example, paw movement appears to be positively correlated with most of the channels, while reward is correlated with channels 5 and 7.

- For the analytic models, the loss function improves roughly by 2% per order up to order 3, then by 1% up to order 7. AIC and BIC are not significant compared to the original loss function for orders up to 10 [fig. 3]. On the contrary, the model evidence, as estimated by the Penny [31] model, appears to go down dramatically with increasing model order, suggesting log bayesian group factors of the order of -20 for each

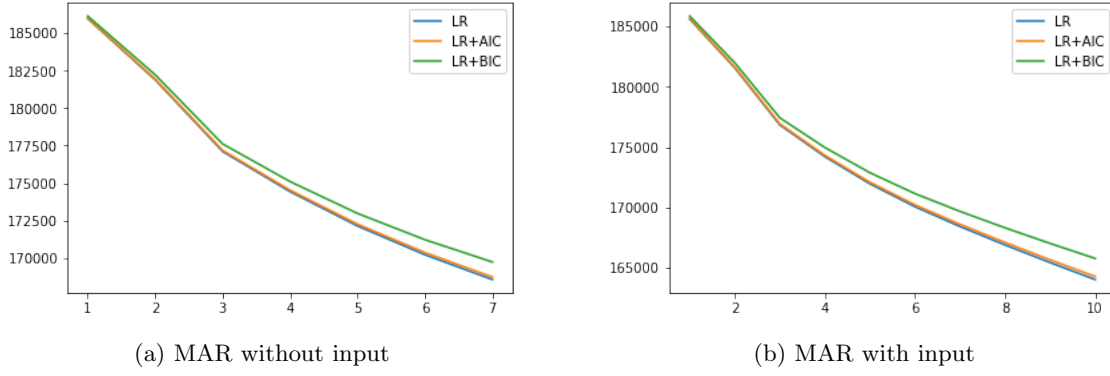(a) MAR without input   (b) MAR with input

Figure 3: Akaike and Bayesian Information Criteria for MAR model fit as a function of model order.
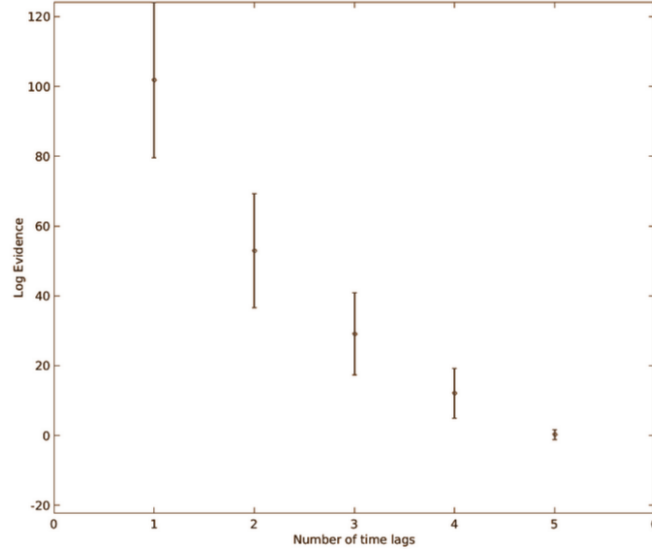

Figure 4: Mean and variance of inter-trial log Model Evidence for MAR model as a function of model order

following model order [fig. 4]. It is likely that at least one of the model selection criteria we have used has a bug, but we are not able to resolve it at this time.

4.1 Linear Classifiability

In this section, we decided to test if the neuronal signals were predictive of mouse performance. For simplicity, we restricted the predictive capacity of the data to that of a linear classifier trained on it. A simple way to test if data is predictive of the associated labels is to set the null hypothesis "It is not possible to predict the labels from the data better than chance", and then test for the level of confidence at which the null hypothesis can be rejected. Firstly, in order to avoid fitting the noise, we performed dimensionality reduction on the data using PCA, and selected only PC's with eigenvalues greater than 10^{-2} [fig. 8]. Then, we trained a binary linear classfier for each of the 4 possible performance outcomes in order to obtain classification accuracy of the true labels. Finally, we permuted the labels multiple times, re-training the classifiers every time. This approach worked nicely for GO and NOGO trials [figs. 10a and 10b]. The number MISS and FA trials form only a very small proportion of the whole trial set, which resulted in high classification accuracies happening by chance. In order to obtain a more rigorous estimate, we proceeded to randomly select a subset of non-MISS trials of number equal to that of the MISS trials, estimate the true and permuted classification accuracies, then repeat the whole process 10000 times. We can conclude that it is possible to construct a classifier identifying GO and NOGO trials from neuronal data with accuracy of the order of 90%, rejecting the null hypothesis with z-scores of the order of 20. For FA it is possible to demonstrate rejection of the null hypothesis with z-score of 3.8, for MISS it is negligible. We conclude that more data is required to make robust statements about accuracy of linear classifiability for MISS and FA trials.

A question more important to this study is whether the performance classes can be predicted from the estimated FC, as that might indicate the use of different neuronal pathways during different behaviour. Inspecting the bulk-trial estimates of A_1 matrices for each performance class by eye, we were able to tell apart small differences, but
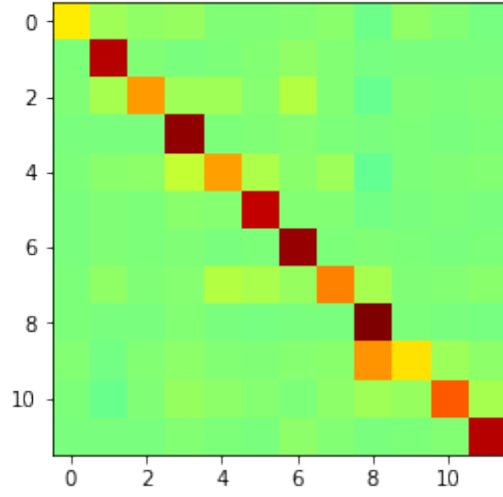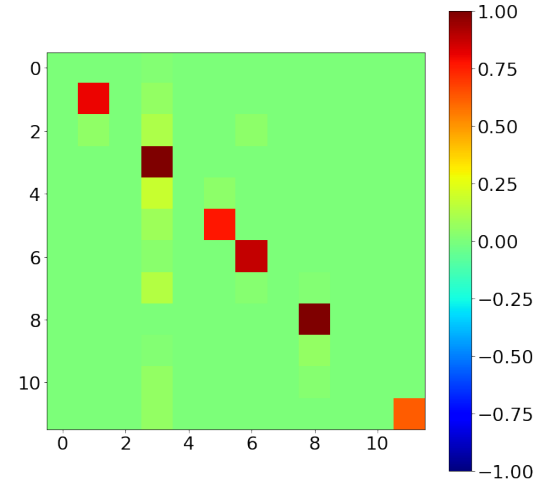
(a) Analytic Estimate Without Input
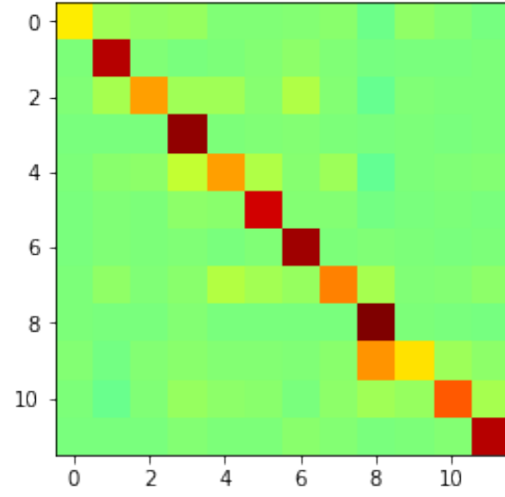
(b) Analytic Estimate With Input
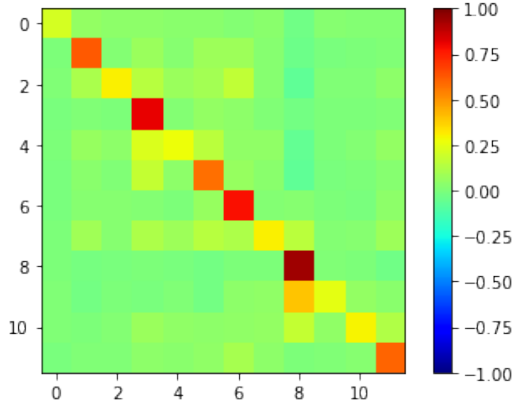
(c) Bayesian Inversion Estimate Without Input

(d) Numeric Regularized Estimate Without Input

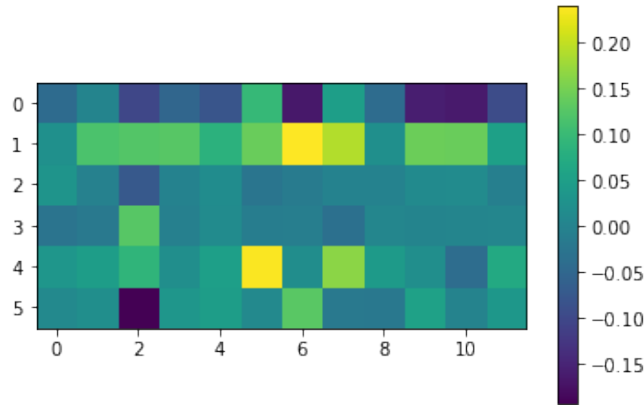Figure 5: MAR A_1 matrices estimated using different approaches to model fitting

Figure 6: Analytic Estimate Of Input Matrix. Horizontal axis denotes neuronal channels, vertical denotes input variables. In order, the input variables are: lick rate, paw movement, starting auditory cue, report auditory cue, reward and first touch
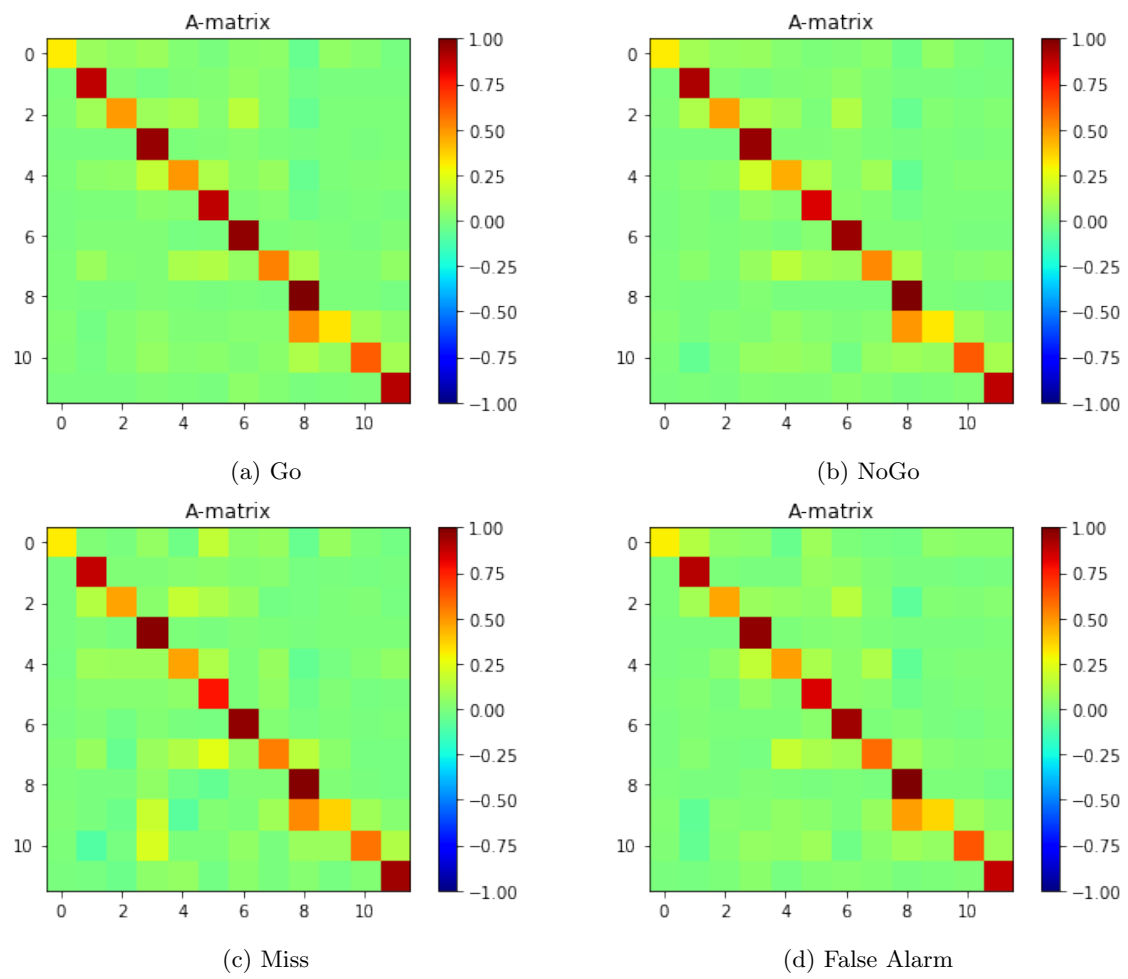
(a) Go

(b) NoGo

(c) Miss

(d) False Alarm

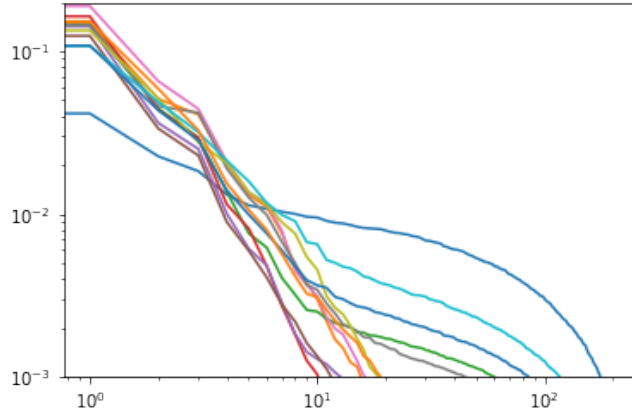Figure 7: MAR A_1 matrix estimates for different performance classes

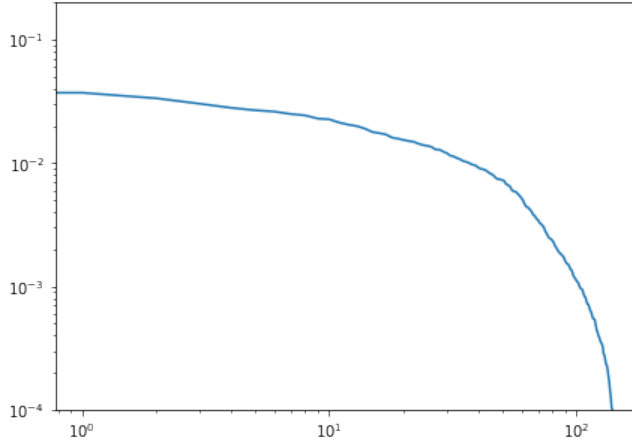Figure 8: Eigenvalue magnitude of neuronal signals of 12 channel mouse. Color denotes individual channels

Figure 9: Eigenvalue magnitude of MAR A_1 matrix

fundamentally they appeared quite similar [fig. 7]. To clarify this question, we repeated the same procedure as for the neuronal signals: dimensionality reduction [fig. 9], followed by true and shuffled linear classification accuracy estimation [fig. 11]. The results are essentially the same as for the neuronal signals. It is very much possible to classify GO and NOGO trials, albeit now the classfication accuracy is 88% and 82% and the z-scores are 14.5 and 9.5 respectively. Our conclusion about the classifiability of MISS and FA trials is the same as for the previous scenario.

5   DCM Model

While I have not found sufficient time to complete this analysis within the given time frame, it is intended to do this analysis for the following publication. For this purpose, I outline the steps necessary for the analysis. In a recent paper [20] Jung et al. have proposed a DCM paradigm to model calcium imaging data. We intend to use their result as a starting point.

5.1   Latent variable model

DCM models make use of two sets of equations - the latent variable equation, which self-consistently models the dynamics of latent variables and external inputs, as well as the forwards model, which computes the observable values based on the latent variables. Typically, DCM models make use of the neuronal state equation [37]

$$\vec{x}(t+1) = A\vec{x}(t) + B\vec{x}(t)\vec{u}(t) + C\vec{u}(t) + \nu, \quad \nu \sim \mathcal{N}(\vec{\mu}, \Sigma) \tag{3}$$

Instead [20] follow the convolution-based model based on the work of Moran et al [26] . The membrane potential of a neuronal population is given by a convolution of a non-linear function of internal and external input with a suitable kernel

$$V_i(t) = h_i(t) \otimes (Inp_i(t) + \Sigma_j \gamma_{ij} \sigma_j (V_i - T_i)) \tag{4}$$

(a) Go. Z-score 21.5

(b) NoGo. Z-score 22.3

(c) Miss. Z-score 0.62

(d) False Alarm. Z-score 3.8
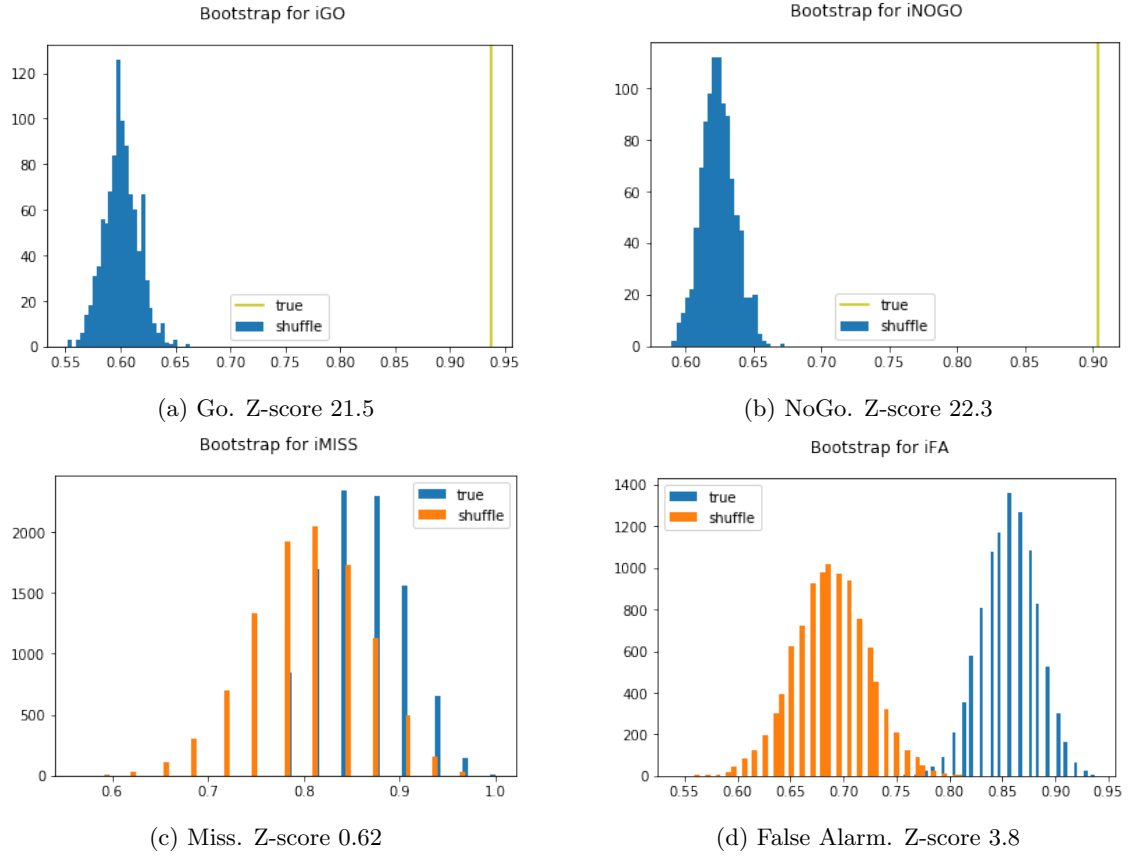
Figure 10: Classifiability of mouse performance from neuronal data

(a) Go. Z-score 14.5

(b) NoGo. Z-score 9.57

(c) Miss. Z-score -0.05
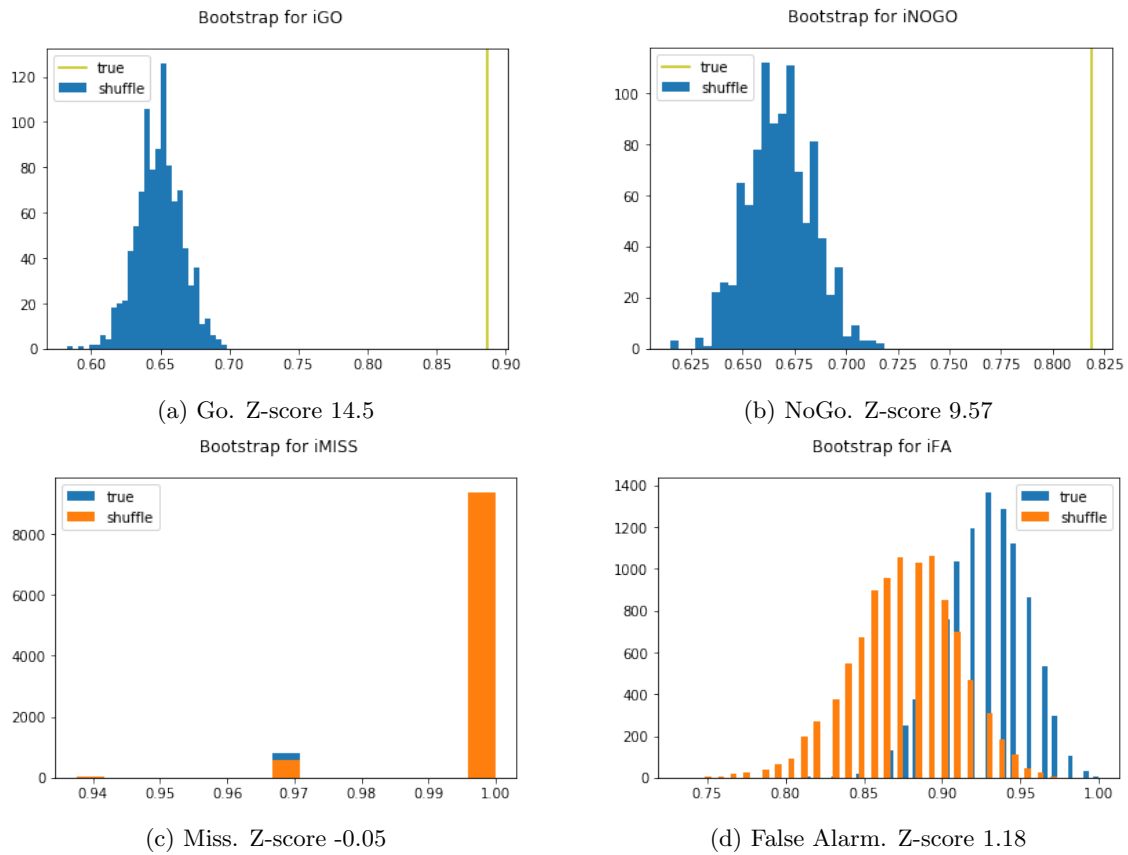
(d) False Alarm. Z-score 1.18

Figure 11: Classifiability of mouse performance from MAR-estimated functional connectivity

where i denotes the index of a neuronal population, $Inp_i(t)$ is the external input to each neuron, γ_{ij} are the connection weights, is the nonlinear activation function, T_i is the firing threshold, the non-linear transfer function is given by

$$\sigma_i(V_i - T_i) = \frac{f_{max}}{1 - e^{R(V_i - T_i)}} \tag{5}$$

and the kernel is given by

$$h_i(t) = H_i k_i t e^{-k_i t} \tag{6}$$

Using differentiation, the above equation can be rewritten in the form of an ODE

$$\dot{V}_i = I_i \tag{7}$$
$$\dot{I}_i = k_i H_i (Inp_i + \Sigma_j \gamma_{ij} \sigma_j (V_i - T_i))) - 2k_i \dot{V}_i - k_i^2 (V_i - T_i) \tag{8}$$

where I is the membrane current. This model is effectively a set of damped harmonic oscillators, coupled together by a nonlinear transfer function.

5.2 Forwards model

Jung et al. [20] use the forwards model designed by Rahmati et al[32] to estimate the calcium signal from the membrane potential.

$$\frac{d}{dt}[Ca^{2+}] = K_{ca} g_{ca} \sigma(V_i - T_i) - \frac{[Ca^{2+}] - [Ca^{2+}]_{base}}{\tau_{ca}} \tag{9}$$

$$F = d_F + k_F \frac{[Ca^{2+}]}{[Ca^{2+}] + k_d} \tag{10}$$

Thus, in the absence of noise, the variables $V(t), I(t)$ and $[Ca^{2+}](t)$ form a deterministic dynamical system, enabling us to compute their values any time in the future given suitable initial conditions.

5.3 Observer noise

The simplest problem in DCM is model inversion under observer noise. Namely, the measured fluorescence is assumed to be sampled from a multivariate normal distribution with some (generally unknown) covariance matrix. The mean of the distribution is then given by the forwards model

$$F_m(t) \sim \mathcal{N}(F(t), \Sigma) \tag{11}$$

In this case, the likelihood function $P[F_m(t)|\theta(t)]$ is given by

$$P[F_m(t)|\theta(t)] = Gau(F_m(t) - F(t, \theta(t)), \Sigma) \tag{12}$$

And the total likelihood of the data.

$$L[F_m|\theta] = \prod_t Gau(F_m(t) - F(t, \theta(t)), \Sigma) \tag{13}$$

The unknown parameters at time t are given by the time-changing latent variables, as well as some unknown constants of the model

$$\theta(t) = \{V(t), I(t), [Ca^{2+}](t), \gamma_{ij}, \tau, ...\} \tag{14}$$

Now, since the $\theta(t)$ are not known, it would make sense to eliminate them from the model. Using the fact that the model is deterministic, we can replace F with an equivalent function $\tilde{F}$, which only requires initial values of parameters to compute the estimate of the observed signal

$$F(t, \theta(t) = \tilde{F}(t, \theta(0)) \tag{15}$$

$\tilde{F}$ is can be computed using the following algorithm

- Initialize the latent variable ODE at time $t = 0$ using provided values of $\theta(0)$
- Forwards-integrate ODE to get values of $\theta(t_i)$ for desired time points $\{t_i\}$
- Evaluate $\tilde{F} = F(t_i, \theta(t_i))$ using the forwards model

5.4 Model Inversion

This is how far we got with the model at the moment. While Jung et al. [20] claim to have used SPM for their analysis, no details of the procedure of model inversion is given in their publication. It is fairly clear that given the complexity of the likelihood function, approximations such as Laplace or mean-field are not not computable analytically. Therefore, a numerical MCMC-like computation of optimal parameters and model evidence appears to be the only feasible solution. However, a brief look at the SPM toolbox seems to suggest that other DCM models implemented in it are using VB approach, although more effort is necessary to understand how exactly it is implemented. Perhaps there exists a numerical method to approximate mean-field integrals from VB approach?

6 Acronyms

AIC	Akaike Information Criterion
BIC	Bayesian Information Criterion
DCM	Dynamical Causal Model
EEG	Electroencephalography
FC	Functional Connectivity
fMRI	Functional Magnetic Resonance Imaging
KL	Kullbeck-Liebler (Divergence)
MAR	Multivariate Autoregressive (Model)
MCMC	Markov Chain Monte Carlo
MI	Mutual Information
ME	Model Evidence
TE	Transfer Entropy
VB	Variational Bayes

References

[1] S.-I. Amari. "Information geometry on hierarchy of probability distributions". In: *IEEE Transactions on Information Theory* 47.5 (July 2001), pp. 1701–1711. ISSN: 00189448. DOI: 10.1109/18.930911.

[2] Pierre-Olivier Amblard and Olivier J. J. Michel. "The relation between Granger causality and directed information theory: a review". In: *Entropy* 15.1 (Dec. 2012). arXiv: 1211.3169, pp. 113–143. ISSN: 1099-4300. DOI: 10.3390/e15010113.

[3] S. Baillet and L. Garnero. "A Bayesian approach to introducing anatomo-functional priors in the EEG/MEG inverse problem". In: *IEEE Transactions on Biomedical Engineering* 44.5 (May 1997), pp. 374–385. ISSN: 00189294. DOI: 10.1109/10.568913.

[4] D. S. Bassett et al. "Dynamic reconfiguration of human brain networks during learning". en. In: *Proceedings of the National Academy of Sciences* 108.18 (May 2011), pp. 7641–7646. ISSN: 0027-8424, 1091-6490. DOI: 10.1073/pnas.1018985108.

[5] John W. Belliveau et al. "Functional cerebral imaging by susceptibility-contrast NMR". en. In: *Magnetic Resonance in Medicine* 14.3 (June 1990), pp. 538–546. ISSN: 07403194, 15222594. DOI: 10.1002/mrm.1910140311.

[6] Richard B. Buxton et al. "Modeling the hemodynamic response to brain activation". en. In: *NeuroImage* 23 (Jan. 2004), S220–S233. ISSN: 10538119. DOI: 10.1016/j.neuroimage.2004.07.013.

[7] Edgar A. DeYoe et al. "Functional magnetic resonance imaging (FMRI) of the human brain". en. In: *Journal of Neuroscience Methods* 54.2 (Oct. 1994), pp. 171–187. ISSN: 01650270. DOI: 10.1016/0165-0270(94)90191-0.

[8] Daniel A. Dombeck et al. "Imaging Large-Scale Neural Activity with Cellular Resolution in Awake, Mobile Mice". en. In: *Neuron* 56.1 (Oct. 2007), pp. 43–57. ISSN: 08966273. DOI: 10.1016/j.neuron.2007.08.003.

[9] Fabrizio Esposito et al. "Independent component model of the default-mode brain function: Assessing the impact of active thinking". en. In: *Brain Research Bulletin* 70.4-6 (Oct. 2006), pp. 263–269. ISSN: 03619230. DOI: 10.1016/j.brainresbull.2006.06.012.

[10] Stefan Frassle et al. "Regression DCM for fMRI". In: *NeuroImage* 155 (July 2017), pp. 406–421. DOI: 10.1016/j.neuroimage.2017.02.090.

[11] Karl J. Friston. "Functional and Effective Connectivity: A Review". In: *Brain Connectivity* 1.1 (Jan. 2011), pp. 13–36. DOI: 10.1089/brain.2011.0008.

[12] Ariel Gilad et al. "Behavioral Strategy Determines Frontal or Posterior Location of Short-Term Memory in Neocortex". en. In: *Neuron* 99.4 (Aug. 2018), 814–828.e7. ISSN: 08966273. DOI: 10.1016/j.neuron.2018.07.029.

[13] M. D. Greicius et al. "Functional connectivity in the resting brain: A network analysis of the default mode hypothesis". en. In: *Proceedings of the National Academy of Sciences* 100.1 (Jan. 2003), pp. 253–258. ISSN: 0027-8424, 1091-6490. DOI: 10.1073/pnas.0135058100.

[14] Michael D. Greicius et al. "Persistent default-mode network connectivity during light sedation". In: *Human Brain Mapping* 29.7 (2008), pp. 839–847. DOI: 10.1002/hbm.20537.

[15] J. Gross et al. "Dynamic imaging of coherent sources: Studying neural interactions in the human brain". en. In: *Proceedings of the National Academy of Sciences* 98.2 (Jan. 2001), pp. 694–699. ISSN: 0027-8424, 1091-6490. DOI: 10.1073/pnas.98.2.694.

[16] Daniel Harnack et al. "Topological Causality in Dynamical Systems". en. In: *Physical Review Letters* 119.9 (Sept. 2017), p. 098301. ISSN: 0031-9007, 1079-7114. DOI: 10.1103/PhysRevLett.119.098301.

[17] Anthony Holtmaat et al. "Long-term, high-resolution imaging in the mouse neocortex through a chronic cranial window". en. In: *Nature Protocols* 4.8 (Aug. 2009), pp. 1128–1144. ISSN: 1754-2189, 1750-2799. DOI: 10.1038/nprot.2009.89.

[18] R. Matthew Hutchison et al. "Dynamic functional connectivity: Promise, issues, and interpretations". In: *NeuroImage* 80 (Oct. 2013), pp. 360–378. DOI: 10.1016/j.neuroimage.2013.05.079.

[19] Shinya Ito et al. "Extending Transfer Entropy Improves Identification of Effective Connectivity in a Spiking Cortical Network Model". In: *PLoS ONE* 6.11 (Nov. 2011). Ed. by Michal Zochowski, e27431. DOI: 10.1371/journal.pone.0027431.

[20] Kyesam Jung et al. "Dynamic causal modeling for calcium imaging data reveals differential effective connectivity for sensory processing in a barrel cortical column". In: *bioRxiv* (Jan. 2019). DOI: 10.1101/509653.

[21] H. Kececi and Y. Degirmenci. "Quantitative EEG and cognitive evoked potentials in anemia". fr. In: *Neurophysiologie Clinique/Clinical Neurophysiology* 38.2 (Apr. 2008), pp. 137–143. ISSN: 09877053. DOI: 10.1016/j.neucli.2008.01.004.

[22] Stefan J. Kiebel et al. "Dynamic causal modelling for EEG and MEG". en. In: *Cognitive Neurodynamics* 2.2 (June 2008), pp. 121–136. ISSN: 1871-4080, 1871-4099. DOI: 10.1007/s11571-008-9038-0.

[23] Aaron Kucyi and Karen D. Davis. "Dynamic functional connectivity of the default mode network tracks daydreaming". en. In: *NeuroImage* 100 (Oct. 2014), pp. 471–480. ISSN: 10538119. DOI: 10.1016/j.neuroimage.2014.06.044.

[24] J. T. Lizier and M. Prokopenko. "Differentiating information transfer and causal effect". en. In: *The European Physical Journal B* 73.4 (Feb. 2010), pp. 605–615. ISSN: 1434-6028, 1434-6036. DOI: 10.1140/epjb/e2010-00034-5.

[25] Joseph T. Lizier et al. "Multivariate information-theoretic measures reveal directed information structure and task relevant changes in fMRI connectivity". In: *Journal of Computational Neuroscience* 30.1 (Aug. 2010), pp. 85–107. DOI: 10.1007/s10827-010-0271-2.

[26] Rosalyn Moran, Dimitris A. Pinotsis, and Karl Friston. "Neural masses and fields in dynamic causal modeling". In: *Frontiers in Computational Neuroscience* 7 (2013). ISSN: 1662-5188. DOI: 10.3389/fncom.2013.00057.

[27] Hiroyuki Nakahara and Shun-ichi Amari. "Information-Geometric Measure for Neural Spikes". In: *Neural Computation* 14.10 (Oct. 2002), pp. 2269–2316. DOI: 10.1162/08997660260293238.

[28] S. Nigam et al. "Rich-Club Organization in Effective Connectivity among Cortical Neurons". In: *Journal of Neuroscience* 36.3 (Jan. 2016), pp. 670–684. DOI: 10.1523/jneurosci.2177-15.2016.

[29] S. Ogawa et al. "Brain magnetic resonance imaging with contrast dependent on blood oxygenation." en. In: *Proceedings of the National Academy of Sciences* 87.24 (Dec. 1990), pp. 9868–9872. ISSN: 0027-8424, 1091-6490. DOI: 10.1073/pnas.87.24.9868.

[30] R. D. Pascual-Marqui et al. "Isolated effective coherence (iCoh): causal information flow excluding indirect paths". In: *arXiv:1402.4887 [stat]* (Feb. 2014). arXiv: 1402.4887.

[31] W.D. Penny and S.J. Roberts. "Bayesian multivariate autoregressive models with structured priors". en. In: *IEE Proceedings - Vision, Image, and Signal Processing* 149.1 (2002), p. 33. ISSN: 1350245X. DOI: 10.1049/ip-vis:20020149.

[32] Vahid Rahmati et al. "Inferring Neuronal Dynamics from Calcium Imaging Data Using Biophysical Models and Bayesian Inference". en. In: *PLOS Computational Biology* 12.2 (Feb. 2016). Ed. by Claus C. Hilgetag, e1004736. ISSN: 1553-7358. DOI: 10.1371/journal.pcbi.1004736.

[33] U Sakoglu, Am Michael, and Vd Calhoun. "Classification of schizophrenia patients vs healthy controls with dynamic functional network connectivity". en. In: *NeuroImage* 47 (July 2009), S57. ISSN: 10538119. DOI: 10.1016/S1053-8119(09)70216-2.

[34] Thomas Schreiber. "Measuring Information Transfer". In: *Physical Review Letters* 85.2 (July 2000). arXiv: nlin/0001042, pp. 461–464. ISSN: 0031-9007, 1079-7114. DOI: 10.1103/PhysRevLett.85.461.

[35] A. K. Seth, A. B. Barrett, and L. Barnett. "Granger Causality Analysis in Neuroscience and Neuroimaging". In: *Journal of Neuroscience* 35.8 (Feb. 2015), pp. 3293–3297. DOI: 10.1523/jneurosci.4399-14.2015.

[36] Gergely Silasi et al. "Intact skull chronic windows for mesoscopic wide-field imaging in awake mice". en. In: *Journal of Neuroscience Methods* 267 (July 2016), pp. 141–149. ISSN: 01650270. DOI: 10.1016/j.jneumeth.2016.04.012.

[37] Klaas E Stephan et al. "Dynamic causal models of neural system dynamics: current state and future extensions". en. In: *Journal of Biosciences* 32.1 (Jan. 2007), pp. 129–144. ISSN: 0250-5991, 0973-7138. DOI: 10.1007/s12038-007-0012-5.

[38] Yaroslav Sych et al. "High-density multi-fiber photometry for studying large-scale brain circuit dynamics". en. In: *Nature Methods* 16.6 (June 2019), pp. 553–560. ISSN: 1548-7091, 1548-7105. DOI: 10.1038/s41592-019-0400-4.

[39] Garth John Thompson et al. "Short-time windows of correlation between large-scale functional brain networks predict vigilance intraindividually and interindividually". In: *Human Brain Mapping* 34.12 (June 2012), pp. 3280–3298. DOI: 10.1002/hbm.22140.

[40] Pedro A. Valdes-Sosa et al. "Effective connectivity: Influence, causality and biophysical modeling". In: *NeuroImage* 58.2 (Sept. 2011), pp. 339–361. DOI: 10.1016/j.neuroimage.2011.03.058.

[41] Raul Vicente et al. "Transfer entropy—a model-free measure of effective connectivity for the neurosciences". In: *Journal of Computational Neuroscience* 30.1 (Aug. 2010), pp. 45–67. DOI: 10.1007/s10827-010-0262-3.

[42] Roberto Viviani, Irene Messina, and Martin Walter. "Resting State Functional Connectivity in Perfusion Imaging: Correlation Maps with BOLD Connectivity and Resting State Perfusion". en. In: *PLoS ONE* 6.11 (Nov. 2011). Ed. by Xi-Nian Zuo, e27050. ISSN: 1932-6203. DOI: 10.1371/journal.pone.0027050.

[43] Michael Wibral, Raul Vicente, and Joseph T. Lizier, eds. *Directed Information Measures in Neuroscience*. Springer Berlin Heidelberg, 2014. DOI: 10.1007/978-3-642-54474-3.

[44] J. J. Wright and D. T. J. Liley. "Dynamics of the brain at global and microscopic scales: Neural networks and the EEG". en. In: *Behavioral and Brain Sciences* 19.2 (June 1996), pp. 285–295. ISSN: 0140-525X, 1469-1825. DOI: 10.1017/S0140525X00042679.

[45] Lotfi A. Zadeh and John R. Ragazzini. "An Extension of Wiener's Theory of Prediction". en. In: *Journal of Applied Physics* 21.7 (July 1950), pp. 645–655. ISSN: 0021-8979, 1089-7550. DOI: 10.1063/1.1699725.